Optical Vortices with Starlight: Implications for ground-based stellar coronagraphy

F. Tamburini, G. Anzolin, G. Umbriaco, A. Bianchini, and C. Barbieri

Dipartimento di Astronomia, Università di Padova,
vicolo dell'Osservatorio 3, I-35122 Padova, Italy.

Using an $l = 1$ blazed fork-hologram at the focal plane of the Asiago 122 cm telescope, we obtained optical vortices from the stellar system Rasalgethi (α Herculis) and from the single star Arcturus (α Bootis). We have analyzed the structure of the optical vortices obtained from non-monochromatic starlight under very poor seeing conditions using a fast CCD camera to obtain speckle patterns and carry out the *lucky imaging* technique, alternative to adaptive optics. With the insertion of a red filter and of a Lyot stop we performed $\ell = 1$ optical vortex coronagraphy the double star HD74010. The results are in agreement with theory and numerical simulations. Our results open the way to applications of optical vortices to ground based astronomical observations, in particular for coronagraphy with $\ell > 1$ masks. No intrinsic orbital angular momentum was detected in the starlight.

Introduction – Optical vortices (OVs) are phase defects embedded in light beams endowed with orbital angular momentum (OAM). OVs, and more in general light beams carrying OAM, are generated after the insertion of a phase modulating device (PMD) that imprints a certain vorticity on the phase distribution of the original beam. Such beams can be mathematically described by a superposition of Laguerre-Gaussian (L-G) modes characterized by the two integer-valued indices ℓ and p. The azimuthal index ℓ describes the number of twists of the helical wavefront and the radial index p gives the number of radial nodes of the mode. The electromagnetic field amplitude of a generic L-G mode in a plane orthogonal to the direction of propagation is

$$u_{\ell p}(r,\theta) \propto \left(\frac{r\sqrt{2}}{w_0}\right)^{|\ell|} L_p^{|\ell|}\left(\frac{2r^2}{w_0^2}\right) \exp\left(-\frac{r^2}{w_0^2}\right) \exp(-\mathrm{i}\,\ell\,\theta) \tag{1}$$

where w_0 is the beam radius and $L_n^m(x)$ is the associated Laguerre polynomial. The presence of a phase factor $\exp(-\mathrm{i}\,\ell\,\theta)$ implies that these cylindrically symmetric modes carry an OAM equal to $\ell\hbar$ per photon, relative to their symmetry axis [1, 2]. For the same reason, a phase singularity is embedded in the wavefront, all along the propagation axis, with topological charge equal to ℓ. The intensity distribution of an L-G mode with $p = 0$ is generally shaped as a ring with a central dark hole, where the intensity is null due to total destructive interference. The radius of maximum intensity of this *donut* grows as the square root of ℓ and the intensity value decreases as $\ell^{-1/2}$ [3].

Experimentally, these properties are produced with beams propagating through nonlinear optical systems [4] and Kerr nonlinear refractive media [5]. This induced to argue that OAM could also be naturally generated by some astrophysical environments, possibly related to turbulent interstellar media with density discontinuities on wide scale ranges or to the distorted geometry around Kerr black holes. It was suggested that OAM could be also present in the blackbody radiation of the cosmic microwave background [6]. OVs have been already applied in diverse research fields such as laboratory optics, nanotechnologies and biology [7]. Two astronomical applications have been indicated: first, to overcome the instrumental limitations in the resolution of very close stellar sources due the Rayleigh separability criterion in diffraction-limited telescopes [8, 9, 10], second, to improve the capability of imaging extrasolar planets by peering into the darkness of an OV generated by a PMD inserted in the optical path of a Lyot-type coronagraph [9, 11, 12]. Similar results can be obtained by direct imaging and analysis of tiny deviations of the main star's OV introduced by the presence of a close fainter companion [13, 14]. However, ground-based telescopes will always feel the detrimental effects of atmospheric turbulence (seeing), which reduces the resolving power, even with adaptive optics. Therefore, it is important for the above astronomical applications of OVs to know how the seeing can affect the expected *donut* pattern generated by stellar sources. In this Letter we present the first images of stellar OVs generated by a PMD placed in the optical path of the Asiago 122 cm telescope. In particular, we show how the effects of the atmospheric turbulence can be overcome to produce good quality OVs suitable for OV coronagraphy even under poor seeing conditions and in white light. Even if the contrast needed for the search of exoplanet or for classical coronagraphy can be achieved mainly with even ℓs [15], we decided to use $\ell = 1$ OVs to avoid some experimental complications as higher order ones may not remain stable while propagating in turbulent media, and may split in first order ones [16].

Non-monochromatic optical vortices – Several types of PMDs have been designed to generate axially symmetric OVs from an incident monochromatic on-axis beam. The most efficient are computer-generated fork-holograms [17] and spiral phase plates (SPP) [18]. How-

ever, the use of non-monochromatic beams in astronomical applications of OVs is mandatory to collect enough photons from faint stellar objects. In this case, the *donut*-shaped structure of monochromatic OVs will be changed [19, 20]. Using SPPs, which are helicoidal transmission optical devices with a given total thickness variation h_s, all monochromatic OVs will have the same axis of symmetry. However, different wavelengths will present different OAM values according to $\ell = \Delta n(\lambda) \, h_s/\lambda$, where Δn is the difference between the refraction indices of the SPP material and the surrounding medium. Thus, the transmitted beam will possess different OAM values producing *donut*-shaped patterns of different sizes and a progressive filling of the central dark region. Recently [21] a scheme has been proposed to overcome this problem, but achromaticity is expected only for a limited bandwidth (~ 100 nm) in the visible. We have instead used a fork-hologram which is a grating with a number l of dislocations on its center. Monochromatic on-axis beams produce OVs with OAM indices $\ell = m \, l$, where m is the diffraction order of the grating. Differently from SPPs, fork-holograms present the advantage of generating OVs with the same ℓ at all wavelengths for on-axis polychromatic sources. For off-axis sources ℓ decreases as the star moves away from the center of the hologram.

Spatial coherence of the incident beam is generally assumed to hold only for stellar sources when observed from space, but when ground-based telescopes are used, quite dramatic effects are introduced by the atmospheric turbulence and spatial coherence is lost. However, for exposures shorter than the turbulence timescale ($\sim 10 - 100$ ms in the optical/near-infrared) we can obtain a group of bright speckles that represent the interference image produced by the coherent wavefronts generated by the random distribution of the atmospheric irregularities. A single nearly diffraction-limited stellar image can occasionally be produced when most of the stellar light falls in a single bright speckle. Fried [22] coined the term *lucky exposures* to describe high quality short exposures occurring in such a fortuitous way. This is the basis of *lucky imaging* [23], one of the speckle imaging techniques used in modern astronomy as alternative to adaptive optics. Here we use the *lucky imaging* technique to obtain OVs from stellar sources useful for OV coronagraphy, with the additional restriction of selecting only those exposures where the star to be fainted is centered with the hologram dislocation.

Telescope Observations – Here we report the results obtained in a campaign of observations carried out from 2005 to 2007 with the Asiago 122 cm telescope, that followed some preliminary laboratory simulations [13]. We first observed the multiple system Rasalgethi (α Her) and the single star Arcturus (α Boo). α Her is a visual binary composed by two unresolved binary systems presently separated by $4''.7$: α Her A, formed by an M5 Ib-II semiregular variable ($m_V = 2.7 - 4.0$) and a
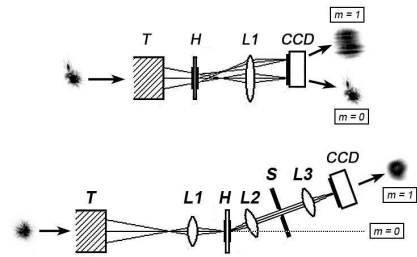

FIG. 1: Optical setups, without (upper panel) and with (lower panel) spatial filter. T is the telescope; *L1, L2, L3* the lenses; H the $l = 1$ fork-hologram; S the spatial filter slit. Stellar speckle patterns are sketched on the left of the optical setups, while the output images at the 0th and 1st diffraction order, on the right. All angles and displacements are exaggerated for clarity.

fainter companion separated by $0''.19$ [24], and α Her B, containing a G0 II-III giant ($m_V = 5.4$) and a fainter secondary separated by $0''.0035$ [25]. α Boo, instead, is a single star having visual magnitude $m_V = 0.04$ and spectral type K1.5 III. We also performed $\ell = 1$ OV coronography with the double system HD74010, which F0 components are separated by $9''.9$ and have visual magnitudes $m_{V,A} = 7.72$ and $m_{V,B} = 7.87$. The optical schemes for the two types of observations to image the OVs are sketched in Fig. 1; the OV coronagraph is presented in [12]. Our $l = 1$ fork-hologram H is blazed at the first diffraction order with 20 lines mm^{-1} and has an active area of 2.6×2.6 mm^2. H was placed in proximity of the F/16 Cassegrain focus of the telescope. The OVs produced by non-monochromatic light beams crossing the fork-hologram show intensity patterns that appear as rings stretched along the dispersion direction with a *central dark strip*. The spectral dispersion also causes a partial filling of the central dark zone. Thus, if we want to use non-monochromatic OVs produced by fork-holograms for OV coronagraphy, we must limit the spectral range [13] and/or restore the *donut* shape (see e. g. [26]). In our case we used a variable spatial filter, S, made by a slit placed on the Fourier plane of the collimating lens *L2* to limit the dispersion of the light at the first diffraction order. This adjustable slit works as a tunable bandpass filter with flat spectral response and has been used only for single on-axis stars. We used a fast CCD camera with 660×494 and 7.4×7.4 μm pixels, 16 bit dynamical range (4000 to 6700 Å with a peak at 5200 Å) to image the OVs' shapes, and, for coronagraphy, the ultrafast EMCCD Andor iXon+ camera.

While observing the multiple system α Her we could simultaneously observe the zeroth and the first diffraction order ($\ell = 0$ and $\ell = 1$, respectively, for on-axis stars). We can then verify how the observed OV patterns change with the distance of the beam from the center of the hologram. We placed the fork-hologram 30 mm
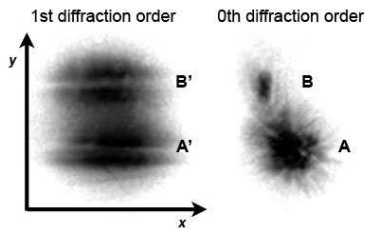
FIG. 2: Speckle pattern (right) and dispersed OVs (left) obtained by summing the 4 *lucky* exposures of α Herculis. The image is displayed in a squared greyscale. The reference system used for the extraction of the OV profiles is reported. The x axis corresponds to the direction of dispersion.

FIG. 3: Observed OV profiles of α Her A (A', left) and α Her B (B', right) obtained from the selected *lucky* exposures. The corresponding numerical simulations are represented by the dotted lines. The thin lines are drown at any dip level.

before the telescope focal plane and set the main star (α Her A) at the center of the optical system. The mean seeing was $\sim 3''.8$. Under such bad seeing conditions the *lucky imaging* technique empirically predicts that the resolution should improve by a factor 2 if we select 1% of frames taken with an exposure time of ~ 80 ms [23]. We then recorded a sequence of 860 frames at a time step of 70 ms. To select the best exposures we imposed the additional restriction that the intensity of the peaks of the α Her A OV were equal, that corresponded to the stellar beam intersecting the center of the hologram. Fig. 2 represents the sum of the 10% *lucky* speckle patterns observed together with their corresponding OVs. Since the signal from α Her A is saturated, an angular resolution of $\sim 1''.5$ was derived from the full width at half maximum (FWHM) of the intensity profile of α Her B. Being the central part of the OV profile of α Her A saturated, the choice of the *lucky* exposures has been made by analyzing the intensity profiles taken across the wings of the dispersed OVs. In Fig. 3 we analyze in detail the OV profiles averaged over 10 pixels wide strips perpendicular to the dispersion, i. e. along the y axis of Fig. 2. We find that the ratio of the two maxima fitted with two Gaussians is $R_{A'} = 0.995 \pm 0.005$ for the on-axis star and $R_{B'} = 0.83 \pm 0.01$ for the off-axis star. We also numerically reconstructed the theoretical intensity profiles of the chromatically dispersed on-axis and off-axis OVs. These profiles present dips with intensity of 82% and 70% respectively. As expected for $\ell = 1$, their central regions can never be totally obscured also under ideal seeing conditions. The profile A' of α Her A shows a central dip of 81%. The OV generated by α Her B, being off-axis, presents an asymmetric shape with a non-integer ℓ value.

The single star α Boo was set at the center of the hologram and the spatial filter S was introduced to produce a nearly-monochromatic circularly symmetric OV. We adopted a slit width of 0.1 mm, corresponding to a 300 Å bandpass width in the visible, that ensured enough S/N ratio for the 70 ms exposures. Since in this case the slit did not allow the simultaneous observation of the speckle patterns at the zeroth diffraction order, we
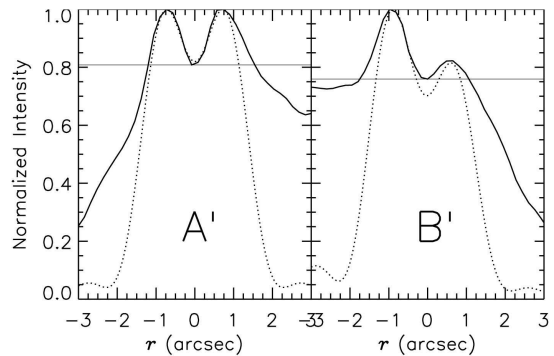
could only select a 17% sub-sample of frames that presented OVs circularly symmetric and therefore centered with the optical singularity of the hologram. We assumed that this condition was met when the ratios of the two intensity peaks measured along two perpendicular axes across the OV were close to 1 within an error of $\sim 10^{-2}$. Fig. 4 shows the OV obtained by summing the selected *lucky* frames. The central region of the OV is not totally dark because of the loss of the starlight coherence due to the very bad seeing conditions and to the presence of residual chromatism. We however notice that the contrast between the dark center and the bright ring improves down to 52% with respect to the previous unfiltered symmetric OVs.

We finally observed the double system HD74010 through a 100 Å bandpass red filter centered at 6532 Å without and with a Lyot stop. The exposure times were 0.01 s. Fig. 5 shows the results of $\ell = 1$ OV coronagraphy: the intensity profiles of the two stars without and with the Lyot mask, obtained by averaging over a 40 pixels strip, are shown in the left panels. Right panels show the corresponding snapshots. The on-axis component B of the binary system appears fainted by a factor ~ 1.7, close to the factor 2 derived from numerical simulations. The partial obscuration of the on-axis star is due to the fact that we were using a $\ell = 1$ fork-hologram. Total obscuration may be mainly achieved with even ℓ values.

Discussion and Conclusions – We demonstrated the feasibility of OV coronagraphy even under very bad seeing conditions with ground-based telescopes. Using the *lucky imaging* technique to improve the quality of our images, we obtained slightly symmetric OV patterns from on-axis starlight beams and performed a first trial of OV coronagraphy obtaining a fainting close to that that can be actually obtained with our $l = 1$ fork-hologram. We tested how the pattern of polychromatic starlight OVs depends from the off-axis position of the star beam. We
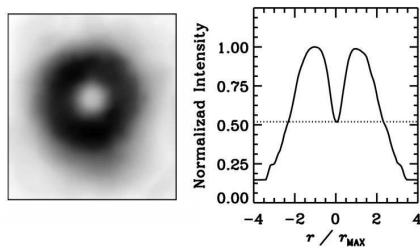
FIG. 4: Left panel: the OV obtained by summing the selected 2% good frames (see text). Left panel: profile of the OV across the direction perpendicular to the dispersion.
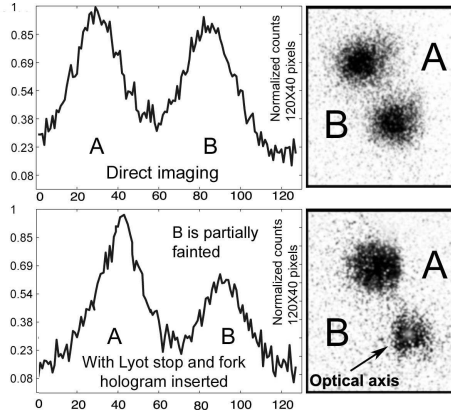

FIG. 5: $\ell = 1$ OV coronagraphy of HD74010. Left panel: the averaged intensity profiles of the double star before (up) and after (down) the insertion of the Lyot stop. Right panel: the corresponding snapshots (see text).

showed how polychromaticity and the lack of coherence produced by the atmospheric turbulence may heavily alter the theoretical *donut* profile of the OV reducing the contrast needed for coronagraphy. Although only even values of ℓ can produce perfect rejection of the on-axis starlight as required for coronagraphy, we decided to start with an $l = 1$ fork-hologram to ensure the stability of the OVs along the optical path. This explains the importance of this choice as a first test of OV coronagraphy. We found that our experimental results are consistent with theoretical predictions. We suggest that these new promising techniques could find their best application mainly at telescopes with adaptive optics, or in space instruments. Finally, since we did not detect any OV at the other diffraction orders of the hologram, we can conclude that starlight does not have an appreciable intrinsic OAM.

[1] L. Allen, M. W. Beijersbergen, R. J. C. Spreeuw, and J. P. Woerdman, Phys. Rev. A **45**, 8185 (1992).
[2] A. Vaziri, G. Weihs, and A. Zeilinger, J. Opt. B **4**, S47 (2002).
[3] M. J. Padgett, and L. Allen, Opt. Commun. **121**, 36 (1995).
[4] F. T. Arecchi, G. Giacomelli, P. L. Ramazza, and S. Residori, Phys. Rev. Lett. **67**, 3749 (1991)
[5] G. A. Swartzlander Jr., and C. T. Law, Phys. Rev. Lett. **69**, 2503 (1992)
[6] M. Harwit, Astrophys. J. **597**, 1266 (2003).
[7] D. G. Grier, Nature **424**, 810 (2003).
[8] D. Palacios, Ph.D. thesis, Worchester Polytechnic Institute, 2004.
[9] G. A. Swartzlander Jr., Opt. Lett. **26**, 497 (2001).
[10] F. Tamburini, G. Umbriaco, G. Anzolin, C. Barbieri, and A. Bianchini, Mem. Soc. Astr. It. Suppl. **9**, 484 (2006).
[11] G. Foo, D. M. Palacios, and G. A. Swartzlander Jr., Opt. Lett. **30**, 3308 (2005).
[12] J. H. Lee, G. Foo, E. G. Johnson, and G. A. Swartzlander Jr., Phys. Rev. Lett., **97**, 053901 (2006).
[13] F. Tamburini, G. Anzolin, G. Umbriaco, A. Bianchini, and C. Barbieri, Phys. Rev. Lett. **97**, 163903 (2006).
[14] C. Barbieri, D. Dravins, T. Occhipinti, F. Tamburini, G. Naletto, V. Da Deppo, S. Fornasier, M. D'Onofrio, R. A. E. Fosbury, R. Nilsson, and H. Uthas, J. Mod. Opt. **54**, 191 (2007).
[15] D. Mawet, P. Riaud, O. Absil, and J. Surdej, Astrophys. J. **633**, 1191 (2005).
[16] J. F. Nye, and M. V. Berry, Proc. R. Soc. A **336**, 165 (1974).
[17] V. Y. Bazhenov, M. V. Vasnetsov, and M. S. Soskin, JETP Lett. **52**, 429 (1990).
[18] M. W. Beijersbergen, R. P. C. Coerwinkel, M. Kristensen, and J. P. Woerdman, Opt. Commun. **112**, 321 (1994).
[19] V. Shvedov, W. Krolikowski, A. Volyar, D. N. Neshev, A. S. Desyatnikov, and Y. S. Kivshar, Opt. Expr. **13**, 7393 (2005).
[20] D. M. Palacios, I. D. Maleev, A. S. Marathay, and G. A. Swartzlander Jr., Phys. Rev. Lett. **92**, 143905 (2004).
[21] G. A. Swartzlander Jr., Opt. Lett. **31**, 2042 (2006).
[22] D. L. Fried, J. Opt. Soc. Am., **68**, 1651 (1978).
[23] N. M. Law, C. D. Mackay, and J. E. Baldwin, 2006, Astron. Astrophys. **446**, 739 (2006). (See also: http://www.ast.cam.ac.uk/~optics/Lucky_Web_Site/).
[24] H. A. McAlister, W. I. Hartkopf, J. R. Sowell, E. G. Dombrowski, and O. G. Franz, Astrophys. J. **97**, 510 (1989).
[25] J. L. Halbwachs, Astron. Astrophys. Suppl. Ser. **44**, 47 (1981).
[26] J. Leach, and M. J. Padgett, New J. Phys. **5**, 154 (2003).